

3D structural imaging of the brain with photons and electrons

Moritz Helmstaedter, Kevin L Briggman and Winfried Denk

Recent technological developments have renewed the interest in large-scale neural circuit reconstruction. To resolve the structure of entire circuits, thousands of neurons must be reconstructed and their synapses identified. Reconstruction techniques at the light microscopic level are capable of following sparsely labeled neurites over long distances, but fail with densely labeled neuropil. Electron microscopy provides the resolution required to resolve densely stained neuropil, but is challenged when data for volumes large enough to contain complete circuits need to be collected. Both photon-based and electron-based imaging methods will ultimately need highly automated data analysis, because the manual tracing of most networks of interest would require hundreds to tens of thousands of years in human labor.

Address

Max-Planck Institute for Medical Research, Department of Biomedical Optics, Jahnstr. 29, D-69120 Heidelberg, Germany

Corresponding author: Helmstaedter, Moritz
(Moritz.Helmstaedter@mpimf-heidelberg.mpg.de)

Current Opinion in Neurobiology 2008, **18**:633–641

This review comes from a themed issue on
New technologies
Edited by Karl Deisseroth and Jeff Lichtman

Available online 9th April 2009

0959-4388/\$ – see front matter

© 2009 Elsevier Ltd. All rights reserved.

DOI [10.1016/j.conb.2009.03.005](https://doi.org/10.1016/j.conb.2009.03.005)

Introduction

Many hypotheses about the brain's network architecture cannot be easily distinguished on the basis of overall functional measurements, such as those based on changes in metabolic demand, or recordings from a small number of cells. Possible network architectures are discussed, for example, in [1] and include modular representation models, such as cell assemblies within cortical columns [2,3], or synfire-chain models [4–7]. Knowledge of the detailed wiring structure could distinguish between these models, which require a distinct synaptic connectivity (Figure 1a). Importantly, these models differ only in their higher order connectivity statistics, which is not revealed by sparse sampling of the network. Complete (dense) mapping of the structure of neural networks has, therefore, received increasing attention over the past years and several methods for neural circuit reconstruction are under development.

Resolution requirements

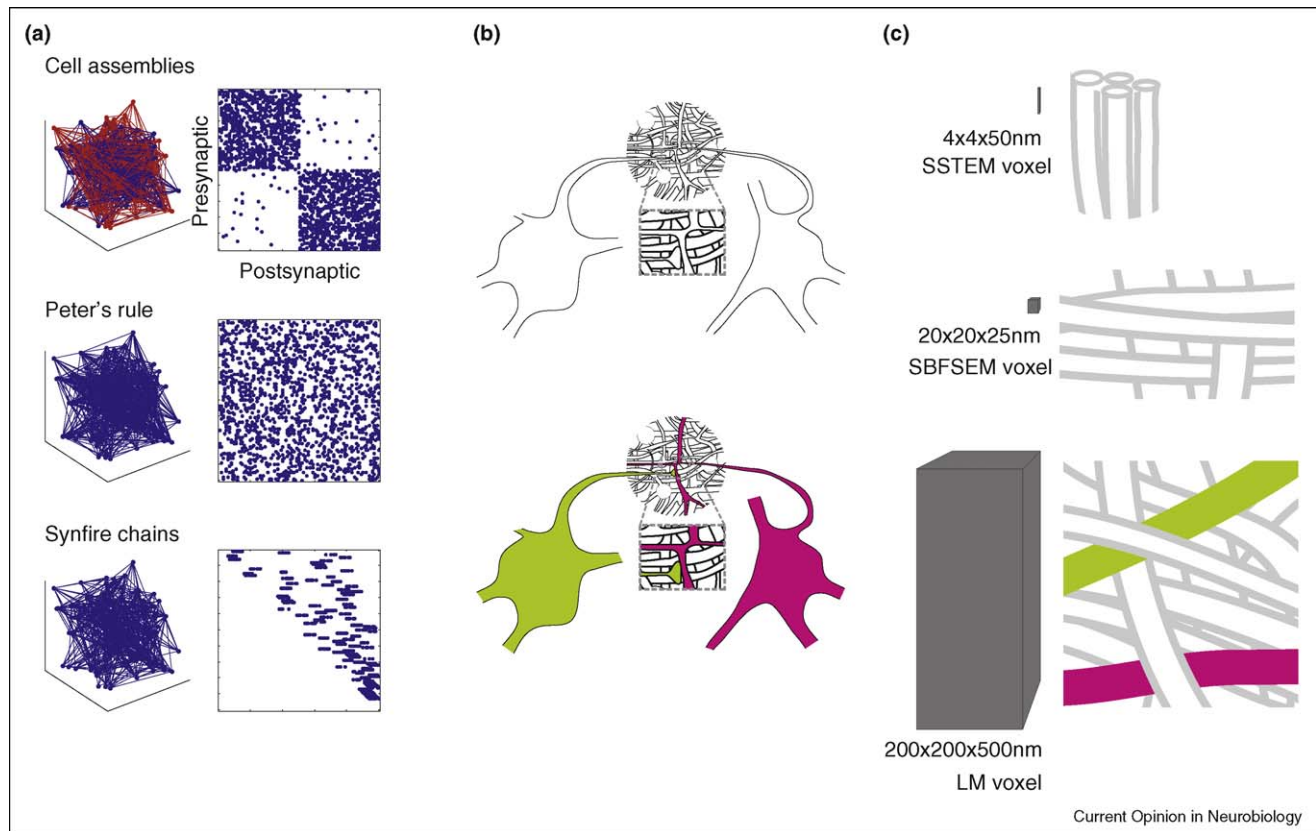
The reconstruction of a complete neural circuit (which can be described by the connection strengths between all possible pairs of neurons) requires for each pair of neurons that first, the somata are identified; second, both axons and dendrites are followed; and third, synapses are detected and their strengths estimated (Figure 1b). If the neurons carry specific labels (e.g. distinct colors), continuity of neurites (but not necessarily their synaptic connectivity, see below) can be inferred from the staining color alone (Figure 1b), allowing for an imaging resolution coarser than the minimum neurite diameter. If the neurons are not specifically labeled, however, then each neurite must be individually resolved. The same applies to synapse identification. If synapses are not specifically stained, characteristic features (such as vesicles, postsynaptic densities, or synapse geometry) have to be spatially resolved. Synapses between a pair of neurons can be inferred directly if the labeling depends on the existence of a synapse (as is the case for *trans*-synaptic virus propagation, see below).

In special cases, such as when axons run in parallel bundles, the imaging resolution can be coarser along the bundle direction than perpendicular to it (Figure 1c, top panel). If, however, the neurite direction can be along any axis in space, as is typical for neuropil, a resolution substantially finer than the minimum neurite diameter is needed along all spatial directions (Figure 1c, middle panel). The imaging resolution can be much lower if specific or sparse staining is employed such that, within a resolution element (voxel) no two neurites from different neurons have the same label (color). The required resolution then depends on the sparseness of the staining and on the number of different labels (Figure 1c, bottom panel). Given a sufficient number of colors even conventional light microscopy (LM) can provide sufficient resolution to follow each neurite even when every cell is labeled. The currently available staining techniques, imaging methods, and reconstruction tools are summarized in Tables 1–3.

Brainbow

The almost complete intracellular staining of a small fraction of all neurons allows neurites to be followed that are too small to be resolved from their neighbors at the light microscopic level. This has been the basis for most cellular neuroanatomy since Ramón y Cajal [8]. The Golgi method [9] and other methods such as biocytin–HRP–DAB staining [10] are monochrome and require that resolution volumes are not shared by different processes, limiting reconstruction to rather sparsely labeled

Figure 1



Topological and geometrical constraints on neural circuit reconstruction. Three types **(a)** of potential connectivity patterns in a set of 100 neurons: cell assemblies (top), locally random connectivity (middle), and synfire chains (bottom). In the wiring diagrams (left), synaptic connections are represented by lines between neurons, in the connectivity matrices (right) by dots at the intersections of the presynaptic (rows) and postsynaptic (columns) neurons. **(b)** Schematic drawing of neuropil where (top) only the membranes are stained and (bottom) two cells in addition with spectrally distinct intracellular labels. Different **(c)** neuropil geometries and staining patterns (right panels) together with the appropriate imaging voxel dimensions shown to the left; neurites in parallel bundles (top), or running in all directions (isotropic, middle). On the bottom, sparsely labeled isotropic neuropil.

tissue. If instead we have a number of *independent* colors one can simply increase the labeling density by that number (*independent* colors, in analogy with primary colors, can be separated by spectral filtering even when voxels contain more than one color). The situation becomes more complicated if we have colors that are merely *distinguishable*, that is, colors that are only distinct as long as a voxel contains just a single color. A small number of *independent* colors can be used to create a large number of *distinguishable* colors. One example is color television (three independent colors), another is the 'rainbow' technology [11,12**] where randomly varied mixtures of up to four spectrally different fluorescent proteins (GFP, YFP, CFP, and RFP) are used to generate about 100 *distinguishable* colors. In analogy to a cable harness containing color-coded wires, this allows the identification of neural processes at both origin and the termination of a neural projection without actually tracing the wires along the harness. For this it is crucial that the color is constant throughout the entire cell. Ideally, each

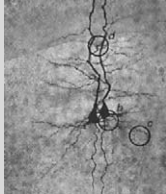
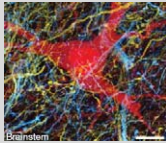
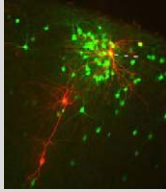
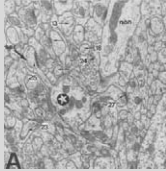
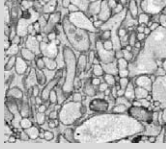
neuron would express a unique color. For the Thy-1 promoter, which is used for the current implementation of brainbow, the fraction of neurons that show expression can be quite variable [13]. Because brainbow colors are not independent a neurite can only be uniquely identified when its diameter exceeds the size of the resolution volume. This is not the case for many nonmyelinated axons [14] and many spines [15] at the resolution of conventional LM. Superresolution LM [16–18] may improve the situation. Synapses can in some — but not all — cases be inferred from the morphology of neurite contacts at the LM level. Synapse-specific immuno-labeling or XFP-labeling might improve the fidelity of synapse identification.

Trans-synaptic tracing

A potentially more reliable method to establish synaptic connectivity is the use of *trans*-synaptic viral infection [19–21], which has recently been improved so as to limit infection to a single retrograde *trans*-synaptic hop [22,23]

Table 1

Staining methods

Method		Applicable imaging methods	Sampling (% of neurons in a given volume)	Order of connectivity resolvable	Reference
Sparse intracellular staining (e.g. biocytin–HRP–DAB)		LM, TEM, SEM	0.001–1% (1–10 of 1000–10000 neurons)	Pairs	[51]
Brainbow		LM	>75% (motor axons, mossy fibers) ^a	∞ for the stained neurons ^b	[12**]
Trans-synaptic tracing		LM	1 postsynaptic neuron, high fraction of presynaptic neurons	High fraction of pairs for a given postsynaptic neuron	[23]
Conventional en-bloc and postsectioning EM stains (osmium, uranyl acetate, and lead citrate)		TEM, SEM	100%	∞	[52] [36]
Surface HRP staining		TEM, SEM	100%	∞^b	[48], KL Briggman, W Denk, unpublished data

Images from [12**,23,51,52]; KL Briggman, W Denk, unpublished data.

^a The neuron sampling ratio for the brainbow technique applies to the current implementation using the Thy1 promoter [12**,13].

^b Assuming that synapses can be identified, discussed in the text.

using a deletion-mutant rabies virus [24] (Table 1). This method works by first transfecting a very sparse set of neurons (using, for example, a gene gun or *in vivo* electroporation) with the DNA encoding a specific receptor for the modified rabies virus, the glycoprotein required for *trans*-synaptic spread (which is missing in the deletion-mutant virus), and DsRed2 as a label for transfected neurons. The virus can then only infect neurons that express the specific receptor. It spreads *trans*-synaptically to a large fraction of presynaptic neurons [20], where the virus genome replicates and expresses EGFP. Lacking the capsule protein, it cannot, however, spread any further. The mechanism of spreading identifies the synapse (if a neuron is *green* it is presynaptic to one of

the *red* neurons) and allows a very efficient sampling of pairwise connectivity for a given postsynaptic neuron. For the technique to become useful for dense reconstruction, it needs to be combined with a method to increase the color space, such as brainbow, and/or with superresolution fluorescence imaging.

Serial section transmission electron microscopy (SSTEM)

The high lateral (*xy*, in-section) resolution of the transmission electron microscope (TEM) in combination with serial sectioning has enabled the reconstruction of neural circuits. Limitations include the painstaking process of manually cutting thousands of sections, and the need for

Table 2

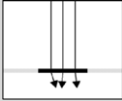
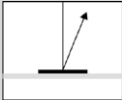
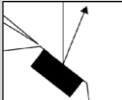
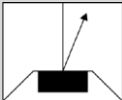
3D-imaging methods			
Imaging method	Cutting method	Voxel size [nm ³]	Number of sequential slices
LM	Optical sectioning	(200–500) ³	For example, 100–300 @ 500–1000 nm for 50–150 μ m of fixed tissue [53]
TEM	 Manual	$\sim 4 \times 4 \times 43\text{--}100$	>8000 @ 50 nm [27] 1200 @ 100 nm [54] 1073 @ 50 nm [28] 214 @ 43 nm [55] 319 @ 90 nm [56] 270 @ 70 nm [45] 200–300 @ 80 nm [57]
SEM	 ATLUM	$\sim 4 \times 4 \times 25\text{--}50$	600 @ 25 nm >1000 @ 35–40 nm (JW Lichtman, personal communication)
	 FIB-SBFSEM	$\sim 4 \times 4 \times 15\text{--}40$	120 @ 40 nm [33**]
	 Diamond-knife SBFSEM	$20 \times 20 \times 25$	2000 @ 25 nm (KL Briggman, W Denk, personal communication)

image alignment (for recent reviews: [25,26]). An even more fundamental problem is that the resolution in the z direction (perpendicular to the sectioning plane), which is determined by the section thickness (≥ 45 nm), is coarser

than that required to follow thin in-plane processes reliably. For thick (>200 nm) neurites or oriented axon tracts a slicing thickness of 45 nm is sufficient. Most published SSTEM studies comprise, at most, a few

Table 3


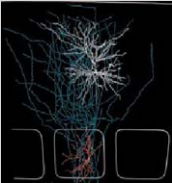
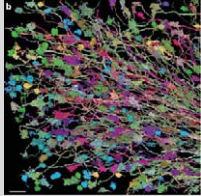
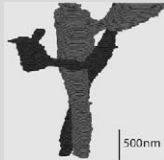
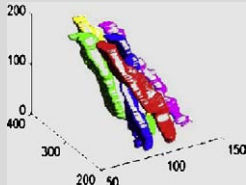
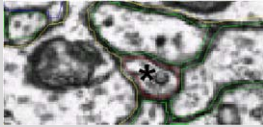
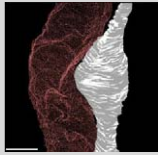
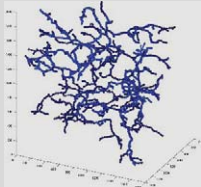
Reconstruction				
Method	Staining–imaging combination	Speed [hours per millimeter neurite length]	Reconstructable total neurite path length (2000 hour human work load) ^a	Reference
Manual volume labeling	 Conventional – TEM	200–400 hours/mm ^b	5–10 mm	[43,58]
	 Single neuron staining – LM	0.25–1 hours/mm ^c	2000–8000 mm	[51,59]

Table 3 (Continued)

Method	Staining–imaging combination	Speed [hours per millimeter neurite length]	Reconstructable total neurite path length (2000 hour human work load) ^a	Reference	
(Semi)automated volume labeling		Brainbow – LM	8–12 hours/mm ^f	170–250 mm	[11,12**]
		Extracellular – SBFSEM	200–400 hours/mm	5–10 mm	M Helmstaedter, KL Briggman, W Denk, unpublished observations
		Brainbow – LM	2 hours/mm	1000 mm	[40–42,60]
		Conventional – SSTEM	40 hours/mm ^d	50 mm	[61]
		Conventional – SBFSEM	5.5 hours/mm ^e	400 mm	[62,63]
Skeletonization		Extracellular – SBFSEM	10–20 hours/mm	100–200 mm	M Helmstaedter, KL Briggman, W Denk, unpublished observations

Reconstruction methods for neural circuit reconstruction. Images from [12**,42,52,59,61,62] and M Helmstaedter, KL Briggman, W Denk, unpublished data.

^a For comparison: 1 cortical column contains approximately 240 000–400 000 mm neurite path length (assuming 12 000 neurons with 20 mm path length, or using volume–density estimates summarized in [1]).

^b Assuming a neurite density of 4.5 km/mm³ of cortex [1] and a tracing speed of one to two hours per μm^3 [43]. Quantification of all volumes and identification of individual synaptic structure can take considerably longer (K Harris, personal communication).

^c D Feldmeyer, personal communication.

^d Tracing speed: 0.2 hour per μm^3 [61].

^e For data from the *Calliphora vicina* outer chiasm: 15 s per image with 15 neurites, slice thickness 50 nm [62].

^f JW Lichtman, personal communication.

hundred sections with section thicknesses between 45 and 100 nm (Table 3). A few studies have used substantially larger numbers of sections. For the reconstruction of the *C. elegans* wiring diagram, [27] and for the neural

plexus of the horseshoe crab eye [28] ~5000 and >1000 serial sections were cut at 50-nm thickness. SSTEM analysis of intracellularly stained cells, in combination with prior LM, has also been used to reliably

identify synaptic structures [29–31], a task for which SSTEM is well suited because the high *xy*-resolution allows the recognition of synaptic vesicles and postsynaptic densities. Tight junctions and gap junctions can only be identified in certain orientations, however.

Automated section collection

Some of the limitations of SSTEM can be overcome by an automatic section-collection process. Sections can be cut with a rotary ultra-microtome and collected continuously onto a carbon-coated polymer tape with the Automated Tape-collection Lathe Ultra Microtome (ATLUM) [32]. The tape precludes viewing in the TEM but modern SEMs with field-emission emitters provide comparable resolution and contrast in back-scattered electron mode [32,33,34,35]; (Briggman, Denk, unpublished data). Automated collection reduces the likelihood of lost or damaged sections and appears to reduce section distortion during imaging, presumably because of the supporting substrate (JW Lichtman, personal communication). ATLUM also, for reasons poorly understood so far, allows a reduction of the section thickness to about 25 nm, maybe even less (JW Lichtman, B Kasthuri, personal communication). Sections can be stained using standard contrasting protocols [36] and remain available for repeated imaging, potentially even for postembedding labeling with antibodies [35].

Block-face imaging

Section distortion is one of the main problems preventing the assembly of high-quality 3D EM data. Distortion (and the need to collect sections) can be avoided if each slice is imaged before sectioning. This requires imaging the block face of an embedded sample with sufficient resolution and depth discrimination, which is possible with scanning electron microscopy (SEM), using back scattered-electron detection and low beam energies to limit the electron penetration depth [34]. At a beam energy of 3 kV the sample composition affects the signal down to a depth (information depth) of about 25 nm [37]. To obtain 3D data, the block-face needs to be repeatedly imaged, with the top slice removed in between image acquisitions. One possibility to remove the top slice is the introduction of an ultra-microtome into the chamber of the SEM [38]. Stacks of thousands of images have been acquired with this Serial Block-Face Scanning Electron Microscope (SBFSEM [34]). Diamond-knife SBFSEM currently allows a slice thickness as thin as 25 nm (Briggman, Denk, in preparation), sufficient *z*-resolution to trace any neurite. Although 25 nm slices have been reported with both ATLUM and SBFSEM, it appears difficult to reliably obtain sections below 25 nm (KL Briggman, unpublished data; JW Lichtman, personal communication). Whether thinner sections can at all be cut repeatedly and reliably with a diamond knife is currently unknown. The removal of material in smaller increments is, however, possible with focused ion-beam (FIB) milling [39]. This approach

is also less sensitive to electron-beam-induced damage to the resin, which affects cutting in diamond-knife SBFSEM [34] (Briggman, Denk, unpublished data). The insensitivity to beam damage allows the use of higher electron doses and hence higher resolution and a better signal-to-noise ratio. Knott *et al.* [33] thus were able to record images at a lateral resolution of 4 nm, with good visibility of synaptic vesicles and densities. A crucial issue is the uniformity of the section thickness. Often only the microtome advance or the mitochondria thickness are reported, both of which are not sensitive to variations of the section thickness between subsequent cuts. Cutting problems are often apparent in resliced images along the *z*-direction.

The size of the volume that can be imaged depends, of course, on the number of sections that can be taken in unbroken sequence. It also depends on the block-face area that can be imaged. With ATLUM and diamond-knife SBFSEM one limitation is the width of the diamond knife, which can, however, be several millimeters. In FIB-based SBFSEM the block-face area is currently limited by what can be milled off in a reasonable time and without artifacts, such as surface ripple [33]. For large block faces the imaged area needs to be divided into multiple tiles because of the limited field of view (because of scan-generator restrictions and off-axis electron-optical aberrations) of the SEM at high resolution. The acquisition of well-aligned 3D image stacks with sufficient resolution to trace most neurites has been demonstrated with diamond-knife SBFSEM (Briggman, Denk, unpublished observations) and appears feasible with ATLUM and FIB-SBFSEM.

Reconstruction

The ultimate aim of imaging the structure of neural circuits is to construct neural connectivity matrices (Figure 1a). To achieve this, neurites must be traced through 3D data and synapses between neurites need to be detected and their strength estimated (Tables 1 and 2). A major challenge is following neurites through neuropil with high reliability (Figure 1b). That the human visual system can perform this task demonstrates that the raw data contains sufficient information. Manual tracing can yield valuable insight, but it is time consuming. At the LM level, it takes 0.25–1 hour per mm neurite path length (D Feldmeyer, personal communication). Thus it takes roughly 30 hours to completely trace all neurites belonging to a single intracellularly stained spiny stellate neuron in L4 of rat barrel cortex. Some semiautomated techniques mimic the manual labeling procedure by inferring new contours from already drawn contours in adjacent slices [40–42].

Manual reconstructions from SSTEM image stacks are even slower (one to two hours per μm^3 of gray matter, [43], i.e. 200–400 hours per mm neurite path length,

assuming a neurite density of 4.5 km/mm^3 [1]). Without alternative, manual reconstruction has been used in a number of heroic reconstruction efforts, such as, over a period of 15 years (JG White, personal communication, [26]) virtually the entire nervous system of *C. elegans* [27] (see also [44]). SSTEM-based manual reconstructions of small volumes, $\sim(10\text{--}20 \mu\text{m})^3$ of neural tissue are mostly used to explore details of synaptic structure or of neuron–glia interaction (e.g. [14,45,46]) sometimes in correlation with LM (e.g. [29,31]). For the analysis of complete neuronal wiring diagrams, manual reconstruction of SSTEM images appears to be prohibitively expensive in terms of human labor (24 000–80 000 work years for a cortical column, cf. Table 3).

High contrast and the minimization of fixation artifacts are crucial even for entire manual reconstructions. Staining strategies designed to emphasize the cell surface can further aid manual reconstruction and are likely to be necessary for automatic techniques. Surface staining makes it easy to follow the unstained cell lumen through the volume and can be achieved by the infiltration of horseradish peroxidase (HRP) into the living tissue followed by fixation and a standard DAB staining and OsO_4 enhancement protocol [47] or by genetically targeting HRP to cell membranes [48].

Well-aligned 3D data from cell surface-stained material are promising for computer-based segmentation methods not only because of the high contrast but also because of the availability of an undistorted surround in all three dimensions. This makes this problem amenable to machine-learning-based analysis such as memory-based pattern matching (Helmstaedter, Briggman, Denk, unpublished data), convolutional neural network classifiers [49], or hierarchical random-forest classifiers [50]. Crucial for any machine-learning method is the availability of high-quality training data (Helmstaedter, Briggman, Denk, unpublished data) and of test data that can evaluate the reliability of automatically generated segmentations over longer distances. The training data are best generated using careful tracing of a small volume. To test its performance, it is crucial to know whether an automatic segmentation procedure correctly predicts whether two distant points belong to the same neurite or not. This can be tested using manually generated skeletons (tree-like structures comprising lines running roughly along the centers of neurites). Given appropriate software tools (Table 3), skeletons can be generated in SBFSEM data at a speed of approx. 15 hours per mm neurite path length (Helmstaedter, Briggman, Denk, unpublished data), which is more than 10 times faster than volume labeling. The figure-of-merit for any algorithm will not be so much the speed at which it runs on the computer but, rather, by which factor it reduces the total human workload, including any proofreading and error-correction steps. To make the complete reconstruction of,

for example, a cortical column feasible (1 work year) the workload needs to be reduced several thousand times compared to that needed to manually trace skeletons (1200–4000 work years for a cortical column, Table 3). To us the increase of the analysis speed seems much more important than speeding up acquisition. Even with SBFSEM, where voxel rates are currently limited to well below a megavoxel/s, mostly by the need to use low beam energies, it should be possible to take data for an entire cortical column ($\sim 300 \mu\text{m} \times 300 \mu\text{m} \times 1000 \mu\text{m}$; nine tera voxels) in fewer than two years. Sufficiently fast analysis will only be possible if the segmentation algorithm is in itself reliable enough or else reliably pinpoints locations where human interaction is needed. The necessary overall reliability depends on the error rate that one is prepared to accept in the connection matrix, which in turn depends on the hypotheses that need to be tested. For a reliability of the cortical-column connectivity matrix of, say, 99% (i.e. accepting that 1% of all neurons contain a tracing error), we need a tracing error rate of fewer than 1 error per 2 m of neurite path length (assuming a neurite path length of $\sim 20 \text{ mm}$ per cortical neuron).

Summary

We have reviewed the techniques currently being developed for imaging the connectivity of neural circuits. For the reconstruction of small neural circuits (up to $100 \mu\text{m}$ on a side) at high resolution, the FIB method looks promising. For the reconstruction of long-range projections, LM-based techniques such as Brainbow or EM-based techniques used on a coarser scale (cutting of $>200\text{-nm}$ -thick slices) are well suited. For the reconstruction of medium-sized local circuits in their entirety (e.g. a $300 \mu\text{m} \times 300 \mu\text{m} \times 100 \mu\text{m}$ volume of retina, or a cortical column) mechanically cutting techniques such as SBFSEM or ATLUM may be the most suitable. Essential but still unsolved is the automated reconstruction of the data.

Acknowledgements

We thank DB Chklovskii, T Euler, KM Harris, V Jain, JW Lichtman, HS Seung, and S Turaga for helpful discussions and HS Seung for comments on the manuscript. We thank A Borst, E Callaway, D Feldmeyer, KM Harris, JW Lichtman, Y Mishchenko, B Sakmann, and I Wickersham for figure contributions.

References and recommended reading

Papers of particular interest, published within the period of review, have been highlighted as:

- of special interest
- of outstanding interest

1. Braitenberg V, Schüz A: *Cortex: Statistics and Geometry of Neuronal Connectivity* Berlin, Heidelberg: Springer; 1998.
2. Mountcastle VB: **The columnar organization of the neocortex.** *Brain* 1997, **120**(Pt 4):701-722.
3. Basole A, White LE, Fitzpatrick D: **Mapping multiple features in the population response of visual cortex.** *Nature* 2003, **423**:986-990.

4. Abeles: *Local Cortical Circuits*. Berlin, Heidelberg, New York: Springer; 1982.
 5. Abeles: *Corticonics: Neural Circuits of the Cerebral Cortex* Cambridge: Cambridge University Press; 1991.
 6. Hahnloser RH, Kozhevnikov AA, Fee MS: **An ultra-sparse code underlies the generation of neural sequences in a songbird.** *Nature* 2002, **419**:65-70.
 7. Diesmann M, Gewaltig MO, Aertsen A: **Stable propagation of synchronous spiking in cortical neural networks.** *Nature* 1999, **402**:529-533.
 8. Ramón y Cajal S: *Histology of the Nervous System*. Oxford, New York: Oxford University Press; 1995.
 9. Golgi C: **Sulla struttura della sostanza grigia del cervello.** *Gazzetta Medica Italiana. Lombardia* 1873, **33**:244-246.
 10. Horikawa K, Armstrong WE: **A versatile means of intracellular labeling: injection of biocytin and its detection with avidin conjugates.** *J Neurosci Methods* 1988, **25**:1-11.
 11. Lichtman JW, Livet J, Sanes JR: **A technicolour approach to the connectome.** *Nat Rev Neurosci* 2008, **9**:417-422.
 12. Livet J, Weissman TA, Kang H, Draft RW, Lu J, Bennis RA, Sanes JR, Lichtman JW: **Transgenic strategies for combinatorial expression of fluorescent proteins in the nervous system.** *Nature* 2007, **450**:56-62.
- Introduction of the brainbow method. A highly promising method, which allows the reconstruction of long-range projections between well-identified neuronal populations at the cellular level.
13. Feng G, Mellor RH, Bernstein M, Keller-Peck C, Nguyen QT, Wallace M, Nerbonne JM, Lichtman JW, Sanes JR: **Imaging neuronal subsets in transgenic mice expressing multiple spectral variants of GFP.** *Neuron* 2000, **28**:41-51.
 14. Shepherd GM, Harris KM: **Three-dimensional structure and composition of CA3→CA1 axons in rat hippocampal slices: implications for presynaptic connectivity and compartmentalization.** *J Neurosci* 1998, **18**:8300-8310.
 15. Bourne JN, Harris KM: **Balancing structure and function at hippocampal dendritic spines.** *Annu Rev Neurosci* 2008, **31**:47-67.
 16. Betzig E, Patterson GH, Sougrat R, Lindwasser OW, Olenych S, Bonifacino JS, Davidson MW, Lippincott-Schwartz J, Hess HF: **Imaging intracellular fluorescent proteins at nanometer resolution.** *Science* 2006, **313**:1642-1645.
 17. Dyba M, Jakobs S, Hell SW: **Immunofluorescence stimulated emission depletion microscopy.** *Nat Biotechnol* 2003, **21**:1303-1304.
 18. Hell SW: **Far-field optical nanoscopy.** *Science* 2007, **316**:1153-1158.
 19. Card JP, Rinaman L, Lynn RB, Lee BH, Meade RP, Miselis RR, Enquist LW: **Pseudorabies virus infection of the rat central nervous system: ultrastructural characterization of viral replication, transport, and pathogenesis.** *J Neurosci* 1993, **13**:2515-2539.
 20. Ugolini G: **Specificity of rabies virus as a transneuronal tracer of motor networks: transfer from hypoglossal motoneurons to connected second-order and higher order central nervous system cell groups.** *J Comp Neurol* 1995, **356**:457-480.
 21. DeFalco J, Tomishima M, Liu H, Zhao C, Cai X, Marth JD, Enquist L, Friedman JM: **Virus-assisted mapping of neural inputs to a feeding center in the hypothalamus.** *Science* 2001, **291**:2608-2613.
 22. Wickersham IR, Finke S, Conzelmann KK, Callaway EM: **Retrograde neuronal tracing with a deletion-mutant rabies virus.** *Nat Methods* 2007, **4**:47-49.
 23. Wickersham IR, Lyon DC, Barnard RJ, Mori T, Finke S, Conzelmann KK, Young JA, Callaway EM: **Monosynaptic restriction of transsynaptic tracing from single, genetically targeted neurons.** *Neuron* 2007, **53**:639-647.
 24. Mebatsion T, König M, Conzelmann KK: **Budding of rabies virus particles in the absence of the spike glycoprotein.** *Cell* 1996, **84**:941-951.
 25. Harris KM, Perry E, Bourne J, Feinberg M, Ostroff L, Hurlburt J: **Uniform serial sectioning for transmission electron microscopy.** *J Neurosci* 2006, **26**:12101-12103.
 26. Briggman KL, Denk W: **Towards neural circuit reconstruction with volume electron microscopy techniques.** *Curr Opin Neurobiol* 2006, **16**:562-570.
 27. White JG, Southgate E, Thomson JN, Brenner S: **The structure of the nervous system of the nematode *Caenorhabditis elegans*.** *Philos Trans R Soc Lond B Biol Sci* 1986, **314**:1-340.
 28. Fahrenbach WH: **Anatomical circuitry of lateral inhibition in the eye of the horseshoe crab, *Limulus polyphemus*.** *Proc R Soc Lond B Biol Sci* 1985, **225**:219-249.
 29. Knott GW, Holtmaat A, Wilbrecht L, Welker E, Svoboda K: **Spine growth precedes synapse formation in the adult neocortex in vivo.** *Nat Neurosci* 2006, **9**:1117-1124.
 30. Somogyi P, Cowey A: **Combined Golgi and electron microscopic study on the synapses formed by double bouquet cells in the visual cortex of the cat and monkey.** *J Comp Neurol* 1981, **195**:547-566.
 31. Trachtenberg JT, Chen BE, Knott GW, Feng G, Sanes JR, Welker E, Svoboda K: **Long-term in vivo imaging of experience-dependent synaptic plasticity in adult cortex.** *Nature* 2002, **420**:788-794.
 32. Hayworth KJ, Kasthuri N, Schalek R, Lichtman JW: **Automating the collection of ultrathin serial sections for large volume TEM reconstructions.** *Microsc Microanal* 2006, **12**(Suppl. 2):86-87.
- A brief description of the ATLUM technique which automates the conventional SSTEM procedure of cutting ultrathin slices from a block of tissue on a rotating lathe microtome for subsequent imaging.
33. Knott G, Marchman H, Wall D, Lich B: **Serial section scanning electron microscopy of adult brain tissue using focused ion beam milling.** *J Neurosci* 2008, **28**:2959-2964.
- This study explores the use of focused ion-beam milling for serial block-face scanning electron microscopy and may be the technique of choice for the complete reconstruction of small volumes (less than 100 μm on a side) at high resolution.
34. Denk W, Horstmann H: **Serial block-face scanning electron microscopy to reconstruct three-dimensional tissue nanostructure.** *PLoS Biol* 2004, **2**:e329.
- This article reports block-face scanning electron microscopy using a diamond-knife microtome mounted inside a SEM. This technique is promising for obtaining data on neuronal connectivity matrices from intermediate size volumes of dense neuropil (volumes of several hundred micrometers on a side).
35. Micheva KD, Smith SJ: **Array tomography: a new tool for imaging the molecular architecture and ultrastructure of neural circuits.** *Neuron* 2007, **55**:25-36.
 36. Hayat MA: *Principles and Techniques of Electron Microscopy: Biological Applications*. edn 4. Cambridge: Cambridge University Press; 2000.
 37. Hennig P, Denk W: **Point-spread functions for backscattered imaging in the scanning electron microscope.** *J Appl Phys* 2007, **102**:123101.
 38. Leighton SB: **SEM images of block faces, cut by a miniature microtome within the SEM – a technical note.** *Scan Electron Microsc* 1981, **Pt 2**:73-76.
 39. Heymann JA, Hayles M, Gestmann I, Giannuzzi LA, Lich B, Subramaniam S: **Site-specific 3D imaging of cells and tissues with a dual beam microscope.** *J Struct Biol* 2006, **155**:63-73.
 40. Cai H, Xu X, Lu J, Lichtman JW, Yung SP, Wong ST: **Repulsive force based snake model to segment and track neuronal axons in 3D microscopy image stacks.** *Neuroimage* 2006, **32**:1608-1620.
 41. Zhang Y, Zhou X, Lu J, Lichtman J, Adjero D, Wong ST: **3D axon structure extraction and analysis in confocal fluorescence microscopy images.** *Neural Comput* 2008, **20**:1899-1927.

42. Cai H, Xu X, Lu J, Lichtman J, Yung SP, Wong ST: **Using nonlinear diffusion and mean shift to detect and connect cross-sections of axons in 3D optical microscopy images.** *Med Image Anal* 2008, **12**:666-675.
43. Fiala JC: **Three-dimensional structure of synapses in the brain and on the web.** In *Proceedings of the 2002 International Joint Conference on Neural Networks; May 12-17, Honolulu, Hawaii: 2002:1-4.*
44. Chen BL, Hall DH, Chklovskii DB: **Wiring optimization can relate neuronal structure and function.** *Proc Natl Acad Sci U S A* 2006, **103**:4723-4728.
45. Satzler K, Sohl LF, Bollmann JH, Borst JG, Frotscher M, Sakmann B, Lubke JH: **Three-dimensional reconstruction of a calyx of Held and its postsynaptic principal neuron in the medial nucleus of the trapezoid body.** *J Neurosci* 2002, **22**:10567-10579.
46. Witcher MR, Kirov SA, Harris KM: **Plasticity of perisynaptic astroglia during synaptogenesis in the mature rat hippocampus.** *Glia* 2007, **55**:13-23.
47. Graham RC Jr, Karnovsky MJ: **The early stages of absorption of injected horseradish peroxidase in the proximal tubules of mouse kidney: ultrastructural cytochemistry by a new technique.** *J Histochem Cytochem* 1966, **14**:291-302.
48. Larsen CW, Hirst E, Alexandre C, Vincent JP: **Segment boundary formation in Drosophila embryos.** *Development* 2003, **130**:5625-5635.
49. Jain V, Murray JF, Roth F, Turaga S, Zhigulin V, Briggman KL, Helmstaedter M, Denk W, Seung HS: **Supervised Learning of Image Restoration with Convolutional Networks.** in *IEEE 11th International Conference on Computer Vision. ICCV; 2007.*
50. Andres B, Köthe U, Helmstaedter M, Denk W, Hamprecht F: **Segmentation of SBFSEM volume data of neural tissue by hierarchical classification.** In *Pattern Recognition.* Edited by Rigoll G; 2008, 5096/2008:142-152.
51. Markram H, Lubke J, Frotscher M, Roth A, Sakmann B: **Physiology and anatomy of synaptic connections between thick tufted pyramidal neurones in the developing rat neocortex.** *J Physiol* 1997, **500(Pt 2)**:409-440.
52. Harris KM, Stevens JK: **Dendritic spines of rat cerebellar Purkinje cells: serial electron microscopy with reference to their biophysical characteristics.** *J Neurosci* 1988, **8**:4455-4469.
53. Tsai PS, Friedman B, Ifarraguerri AI, Thompson BD, Lev-Ram V, Schaffer CB, Xiong Q, Tsien RY, Squier JA, Kleinfeld D: **All-optical histology using ultrashort laser pulses.** *Neuron* 2003, **39**:27-41.
54. Sims SJ, Macagno ER: **Computer reconstruction of all the neurons in the optic ganglion of Daphnia magna.** *J Comp Neurol* 1985, **233**:12-29.
55. Sorra KE, Mishra A, Kirov SA, Harris KM: **Dense core vesicles resemble active-zone transport vesicles and are diminished following synaptogenesis in mature hippocampal slices.** *Neuroscience* 2006, **141**:2097-2106.
56. Calkins DJ, Sterling P: **Microcircuitry for two types of achromatic ganglion cell in primate fovea.** *J Neurosci* 2007, **27**:2646-2653.
57. Lev DL, Weinfeld E, White EL: **Synaptic patterns of thalamocortical afferents in mouse barrels at postnatal day 11.** *J Comp Neurol* 2002, **442**:63-77.
58. Fiala JC: **Reconstruct: a free editor for serial section microscopy.** *J Microsc* 2005, **218**:52-61.
59. Lubke J, Roth A, Feldmeyer D, Sakmann B: **Morphometric analysis of the columnar innervation domain of neurons connecting layer 4 and layer 2/3 of juvenile rat barrel cortex.** *Cereb Cortex* 2003, **13**:1051-1063.
60. Lu J, Tapia JC, White OL, Lichtman JW: **The interscutularis muscle connectome.** *PLoS Biol* 2009, **7**:e32.
61. Mishchenko Y: **Automation of 3D reconstruction of neural tissue from large volume of conventional serial section transmission electron micrographs.** *J Neurosci Methods* 2009, **176**:276-289.
62. Macke JH, Maack N, Gupta R, Denk W, Scholkopf B, Borst A: **Contour-propagation algorithms for semi-automated reconstruction of neural processes.** *J Neurosci Methods* 2008, **167**:349-357.
63. Jurrus E, Hardy M, Tasdizen T, Fletcher PT, Koshevoy P, Chien CB, Denk W, Whitaker R: **Axon tracking in serial block-face scanning electron microscopy.** *Med Image Anal* 2009, **13**:180-188.